

Effects of nitride precipitation on delta phase formation in additively manufactured nickel superalloys

J.S. Zuback¹, T.A. Palmer^{2,3}

¹Materials Science and Engineering Division, Materials Measurement Laboratory, National Institute of Standards and Technology, Gaithersburg, MD 20899

²Department of Engineering Science and Mechanics, Pennsylvania State University, University Park, PA 16802

³Department of Materials Science and Engineering, Pennsylvania State University, University Park, PA 16802

Abstract

Additively manufactured Inconel 625 is particularly susceptible to the formation of niobium-rich δ -phase precipitates in the interdendritic regions during high temperature exposure. With specific minor alloying element combinations and nitrogen mass fractions on the order of 0.1 %, the formation of δ -phase can be suppressed through the precipitation of nitrides. For example, mass fractions of 0.39 % silicon and 0.03 % titanium led to the precipitation of Z-phase and η -nitrides, which consumed the excess niobium in the interdendritic regions and limited δ -phase formation. Even when holding the material at a temperature of 870 °C for 1000 h, the δ -phase volume fraction was approximately 2 %, which is far below the 6 % level observed in the wrought condition. When the titanium mass fraction was increased to 0.21 % and the silicon mass fraction decreased to 0.05 %, titanium-rich MN nitrides formed within the interdendritic regions instead. Since much of the Nb in these regions was not consumed by the nitrides, δ -phase formation was promoted and reached volume fractions above 10 %. The addition of a hot isostatic pressing step prior to high temperature exposure in both alloys produced a more uniform niobium distribution and minimized δ -phase formation at shorter times. At extended times, trends in the δ -phase volume fractions were similar to those observed in the as-deposited condition, with the initial alloy compositions driving differences in the distribution of excess niobium available for δ -phase formation.

Keywords: Additive manufacturing; Nickel superalloy; X-ray diffraction (XRD); Phase transformations; Precipitates

1. Introduction

Wrought nickel superalloys, such as Inconel 625¹, are susceptible to the nucleation and growth of a Nb-rich, orthorhombic delta (δ) phase on grain and twin boundaries during prolonged exposure to temperatures between approximately 650 °C and 1000 °C [1]. In the binary Ni-Nb system [2], δ -phase is a near-stoichiometric Ni₃Nb intermetallic compound with Nb mole fractions ranging from approximately 24.1 % to 26.5 %. Measurements of δ -phase compositions in commercial superalloys, though, have shown some solubility for Ti, Cr, and Fe, but the total mole fraction of these elements in δ -phase is typically less than 10 % [3]. For Inconel 625 alloy compositions that fall within standard ranges, the equilibrium volume fraction of δ -phase ranges from approximately 5 % to 10 %, and the maximum rate of transformation rate occurs at temperature between approximately 850 °C and 900 °C [4].

The δ -phase precipitates display characteristic needle or platelet morphologies that can serve as crack initiation sites and reduce ductility, fracture toughness, and resistance to hydrogen embrittlement [5-7]. Service conditions are generally avoided within the temperature ranges where the precipitation of this phase is promoted. Specifications defining the maximum allowable Nb content in Inconel 625 and other nickel alloys are also adjusted to reduce the susceptibility to δ -phase formation and to improve performance in different environments and industrial applications. For example, the Nb content in Inconel 718 is adjusted to accommodate different service conditions encountered in the aerospace and petroleum exploration application spaces. In aerospace applications, the maximum Nb mass fraction (5.5 %) is higher than that used in petroleum applications (5.2 %), where the hydrogen embrittlement promoted in corrosive environments is exacerbated by δ -phase formation [8].

During fusion-based additive manufacturing (AM) of Inconel 625, complex solidification and thermal histories [9-11] drive the formation of microstructures and properties that are different from those observed in wrought conditions. Under these processing conditions, alloying elements such as Nb and Mo, segregate into the advancing liquid front during solidification, leading to local chemistry variations in the γ -matrix between dendritic cores and the interdendritic regions [9, 12-14]. Segregation of Nb, in particular, accelerates δ -phase precipitation when AM Inconel 625

¹ Certain commercial equipment, instruments, software, or materials are identified in this paper to foster understanding. Such identification does not imply recommendation or endorsement by the Department of Commerce or the National Institute of Standards and Technology, nor does it imply that the materials or equipment identified are necessarily the best available for the purpose.

material is exposed to temperatures in the range of 650 °C to 1000 °C. Higher phase fractions of δ -phase have been found in AM fabricated materials than those observed in the corresponding wrought material [15]. For example, the manufacturer recommended stress relief heat treatments of laser powder bed fusion AM materials are performed at a temperature of 870 °C [14, 16], and δ -phase was observed within minutes in the segregated regions of the solidification structure that continued to grow for the duration of the heat treatment [17, 18]. Similar observations have been made in other Nb-containing nickel superalloy welds [1, 19], clads [20], and castings [21], in which local enrichment in Nb promotes the formation and growth of δ -phase [10, 15].

Variations in Inconel 625 alloy chemistry can also have a significant impact on the formation of δ -phase and other common Nb-containing precipitates, such as Laves phase, MX-type carbonitrides, and η -carbides (M_6C), during similar solidification-based processes [22-24]. For example, Nb, Si, and C contents dictated the solidification products in Inconel 625 weld overlays placed on low alloy steel plates [24, 25], with low carbon contents leading to the formation of Laves phase and other intermetallic compounds and higher carbon contents promoting carbide formation. These secondary precipitates contain significant amounts of Nb and often influence δ -phase formation during subsequent heat treatments. Precipitation dissolution facilitates δ -phase formation due to local Nb enrichment in adjacent regions, while stable phases reduce the available Nb for δ -phase precipitation.

Secondary phase formation in AM Inconel 625 can vary dramatically with changes in minor alloying elements, with nitrogen having a strong influence [11, 12, 26]. When nitrogen mass fractions reached approximately 0.1 % in materials fabricated by directed energy deposition AM, the precipitation of nitrides was promoted, although the type of nitride depended on the relative amounts of silicon and titanium. With relatively low titanium (0.03 %) and high silicon (0.39 %) mass fractions, tetragonal Z-phase ($CrNbN$), diamond cubic η -nitrides (M_6N), and small amounts of niobium-rich MN nitrides formed. In contrast, only titanium rich MN nitrides were observed with high titanium (0.21 %) and low silicon (0.05 %) mass fractions [26]. The nitrides present in the as-deposited condition remained in the microstructure after hot isostatic pressing (HIP). Similar behavior has been observed in other Inconel 625 materials fabricated using powder bed fusion AM, where the formation of niobium-rich MX ($X=C,N$) precipitates and η -nitrides suppressed δ -phase precipitation during a stress relief heat treatment at a temperature of 870 °C for 1 h [27, 28].

The impact of Nb-containing secondary phases on δ -phase formation was investigated in as-deposited and HIP Inconel 625 AM material with nitrogen mass fractions of approximately 0.1 %. As-deposited material was heat treated at 870 °C to link δ -phase formation in the presence of elemental segregation to differences in nitrides arising from variations in alloy chemistry. Identical heat treatments were performed on the same materials that had been previously subjected to HIP, which eliminated segregation and preserved most secondary phases. The Nb segregation, nitride volume fraction, and δ -phase precipitation were evaluated from microstructural data for up to 1000 h. The results are compared with wrought Inconel 625 to highlight the potential benefits for using AM materials to control δ -phase precipitation. The combination of specific alloy compositions and AM processing is shown to provide pathways for tailoring secondary phase precipitation during prolonged high temperature exposure.

2. Experimental Methods

A coaxial powder-fed, laser-based directed energy deposition process was used to fabricate AM builds from two Inconel 625 powder feedstocks. The builds were deposited using a 4 mm diameter laser operated at a power of 2 kW and a travel speed of 10.6 mm/s. Additional experimental details on feedstock characterization, process parameters, and part geometry can be found elsewhere [11]. The chemical compositions of the as-deposited and representative wrought Inconel 625 materials are listed in Table 1. The AM alloys were designated as low and high Fe based on the measured Fe contents relative to the allowable ranges in the standard material specification [29]. The alloy designations are used strictly for consistent nomenclature with previous work [11, 12, 26] and do not suggest any influence on material behavior. Equilibrium thermodynamic calculations were made using ThermoCalc Software [30] with the TCNI8 commercial Ni-alloys database [31] using the respective alloy compositions listed in Table 1 as input. Reported values represent the average and standard deviation in the temperature range of (870 ± 10) °C to account for uncertainty in calculations. Selected portions of both AM materials were also subjected to a standard HIP post-processing [32] performed at a temperature of (1163 ± 25) °C and a pressure of 101 MPa for 4 h.

Prior to heat treatment, as-deposited and HIP samples were wrapped in commercially pure tantalum foil and sealed in 102 mm x 152 mm and 0.05 mm thick 309 austenitic stainless steel bags. All heat treatments were performed in a tube furnace at a temperature of (870 ± 2) °C, which was monitored with a type K thermocouple, for times ranging from 0.5 h to 1000 h. Samples were

removed from the furnace and air-cooled to room temperature. The samples were sectioned in the transverse orientation with respect to the build direction to reveal a fresh surface with no heat treatment scale and then mounted in conductive epoxy. For X-ray diffraction experiments, samples were ground and polished to a 1 μm finish. Samples characterized using electron microscopy were subjected to an additional vibratory polishing step for 4 h using 0.05 μm colloidal silica.

Identification of the individual phases in each sample was performed using a laboratory scale X-ray diffraction (XRD) system equipped with a 2D area detector and a Cu-K α radiation source operated at a voltage of 50 kV and current of 1000 mA. Diffraction patterns were acquired using a 0.6 mm slit and 0.5 mm collimator in the 2θ range of 30° to 60° with a step size of 0.02° and a counting time of 5 s per step. The sample stage was oscillated with an amplitude of 1 mm in orthogonal directions parallel to the sample surface to increase the number of grains probed during each step. Individual diffraction peaks were fit using a Pseudo-Voigt function, and peaks were then indexed from their 2θ positions using powder diffraction files from the Inorganic Crystal Structure Database of the National Institute of Standards and Technology [33].

Precipitate morphologies and compositional variations were characterized using scanning electron microscopy (SEM) combined with energy dispersive spectroscopy (EDS). Secondary electron images were first acquired from sample surfaces that were electrolytically etched for approximately 5 s at 3.5 V with 10 % aqueous chromic acid to reveal precipitates. Volume fractions of δ -phase and other secondary phases were then measured based on precipitate morphology using the point count method [34] by analyzing five images across a total area of approximately 0.9 mm^2 on each sample surface. Precipitates with a needle-like appearance were classified as δ -phase while irregular and blocky particles were assigned as nitrides. Different types of nitrides could not be distinguished by the point count method, but the total nitride volume fraction was measured. Local chemistry variations in the interdendritic regions and dendrite cores were quantified from X-ray spectra obtained using a counting time of 30 s and acquired from 1 μm diameter acquisition points across areas with fields of view of approximately $36 \mu\text{m}$ by $48 \mu\text{m}$. For each field of view, 10 acquisition points located in the interdendritic and dendritic core regions were probed. The mass fractions of metallic elements measured in two fields of view for each material condition were normalized, outliers were removed from the analysis, and the location-specific data were averaged with the standard deviation reported.

3. Results and Discussion

3.1 As-deposited and HIP microstructures

Solidification structures in the as-deposited Inconel 625 alloys exhibited columnar dendrites with precipitates decorating interdendritic regions, which are highlighted in Figure 1(a) and Figure 1(b) for the low and high Fe materials, respectively. In both materials, areas representative of alloying element segregation and the precipitation of secondary phases can be easily identified. Regions of light and dark contrast, corresponding with areas of alloying element segregation, were visible, with the darker regions corresponding to the dendrite cores and the lighter regions to interdendritic regions. The measured local variations in average mass fractions of selected alloying elements across these different regions are tabulated in Table 2.

There was significant enrichment in Nb and Mo within the interdendritic regions of both alloys over that observed in the dendrite core regions. The interdendritic regions in the high Fe alloy are significantly enriched, with the measured (6.19 ± 0.84) % Nb mass fraction approximately 1.5 times than that of the bulk composition and three times higher than that observed in the dendrite cores $((2.02 \pm 0.27) \%)$. In contrast, the measured Mo and Nb compositions in the interdendritic regions of the low Fe alloy were similar to those obtained from bulk measurements, while the dendrite cores contain lower mass fractions of each alloying element.

The enrichment of alloying elements in the interdendritic regions can also promote the formation of secondary phases during solidification [22]. Strong nitride forming elements like Nb, Mo, and Si in the Inconel 625 alloys segregate to the liquid during the terminal stages of solidification, while matrix stabilizing elements like Ni, Cr, and Fe are trapped within the dendrite cores during the early stages of solidification. Precipitates observed in these enriched interdendritic regions in each material are summarized in Table 3 [26]. Previous characterization revealed that various nitride phases arising from differences in the Si and Ti mass fractions in the initial alloy chemistries [11, 12, 26] are prominent across the two alloys, and no δ -phase was observed in the as-deposited condition.

All nitrides observed in these interdendritic regions contained Nb mass fractions in excess of 35 %. Enrichment in other metallic elements was dependent on the type of nitride that forms. In the alloy with relatively low Si and high Ti mass fractions, only MN nitrides were observed with a volume fraction of (1.1 ± 0.2) % measured in the as-deposited condition. In the alloy containing relatively high Si and low Ti mass fractions, Z-phase, η -nitrides, and a small amount

of MN nitrides were identified. When the volume fractions of the nitrides were combined, a cumulative volume fraction of $(2.3 \pm 0.4) \%$ was measured.

These, and other AM fabricated alloys, are also commonly subjected to HIP to reduce porosity and alter microstructures [9]. Since the holding temperature was above the δ -phase solvus temperature, δ -phase did not form in either alloy during HIP. As shown in Figure 1(c) and Figure 1(d), however, the HIP post-processing step eliminated the solidification structure in both the low and high Fe as-deposited materials, respectively. The location and alignment of secondary phases in Figure 1(c) and Figure 1(d) were used to determine the approximate locations of interdendritic regions and dendrite cores prior to HIP. The elemental segregation in the as-deposited microstructure, particularly for Mo and Nb, was eliminated as shown in Table 2, where the compositions in the dendrite cores and interdendritic regions reached similar values that fell within the measurement uncertainty.

Even though elemental segregation in the as-deposited materials was minimized after HIP post processing, many of the various nitrides observed in the as-deposited condition did not transform into new phases and remained in similar locations. Although the MN nitrides in the low Fe alloy were not observed after HIP, the MN nitrides in the high Fe material remained and the average composition became more enriched in Ti, as summarized in Table 3 [26]. No appreciable differences were measured in the compositions of Z-phase and η -nitrides in the low Fe material, and only slight changes in lattice parameters were measured. Precipitates present in both alloys coarsened after the HIP post-processing step, as shown in Figure 1(c) and Figure 1(d). Volume fractions of the nitrides remained largely unchanged, with the volume fraction of MN nitrides in the high Fe material being $(1.0 \pm 0.2) \%$ and the volume fraction of Z-phase and η -nitrides in the low Fe material reaching $(2.6 \pm 0.7) \%$

3.2 Evolution of δ -phase in Inconel 625 containing MN nitrides

When the as-deposited alloys containing primarily MN nitrides were exposed to high temperatures, elemental segregation of Nb and Mo in the interdendritic regions led to the precipitation of additional Nb-containing phases. The precipitation of these Nb-containing phases was accelerated since the elemental segregation alters the local thermodynamic equilibrium and kinetic conditions. The rather sharp drop in Nb mass fractions in the interdendritic regions with increasing time at temperature highlighted in Figure 2(a) shows that Nb was quickly consumed by these newly formed secondary phases, which are shown in Figure 3. After only 0.5 h of exposure,

significant precipitation of needle-shaped δ -phase packets was evident. To a lesser extent, globular MN nitride particles, which are highlighted by arrows in the Nb-enriched interdendritic regions in Figure 3(a), were also evident. Figure 4(a) confirms the presence of both phases after this relatively short high temperature exposure time.

Since both δ -phase and MN nitrides consume Nb during growth, a decrease in the mass fraction of Nb was measured in the interdendritic regions with increasing time, as shown in Figure 2. The average Nb mass fraction decreased from (6.19 ± 0.84) % to (4.50 ± 0.44) % in the interdendritic regions after 1 h, while the Nb levels in the dendrite cores were largely unchanged. As the Nb in the interdendritic regions was consumed by these newly formed precipitates, the volume fraction of secondary phases increased substantially, as shown in Figure 5. Even after just 0.5 h at a temperature of 870 °C, the volume fraction of δ -phase rapidly increased to (3.1 ± 2.8) %, as did the volume fraction of MN nitrides, which increased from (1.1 ± 0.2) % in the as-deposited condition to (3.1 ± 0.2) %.

With increasing time, the mass fraction of Nb in the interdendritic regions decreased as it was consumed by the formation of δ -phase and MN nitrides, which is monitored in Figure 4(a). As additional δ -phase reflections appeared, the corresponding δ -phase volume fraction also increased. The formation of an increasing number of densely packed δ -phase packets in the interdendritic regions with increasing times up to 100 h was confirmed in Figure 3, with the δ -phase volume fraction reaching a peak level of (27.5 ± 4.3) %. After 100 h of heat treatment, however, the Nb composition in the interdendritic regions dropped to a level equal to that in the γ -matrix, hindering further growth of the δ -phase. As a result, the δ -phase clusters became less densely packed, as shown in Figure 3(g) and Figure 3(h), and the amount of δ -phase began to decrease with increasing hold times until a final volume fraction of (10.0 ± 2.9) % was reached after 1000 h. Longer hold times had little effect on the evolution of MN nitrides, with the volume fraction of (3.7 ± 0.9) % measured after 0.5 h remaining largely unchanged up to 1000 h, as seen in Figure 5.

After subjecting the as-deposited material to a HIP post-processing step, an expected reduction in elemental segregation was observed, as shown in Figure 2(b). While the MN nitrides initially observed in the interdendritic regions in the as-deposited material were preserved, they became more enriched in titanium and depleted in niobium. The MN nitrides are the primary precipitates that form in the early stages of heat treatment at 870 °C, as shown in Figure 6(a)-(d),

due to the decrease in elemental segregation arising from the HIP post-processing step. There was an immediate increase in the volume fraction of these MN nitrides to (1.9 ± 0.6) % after 0.5 h, as shown in Figure 5(a), but the volume fraction stabilized after 10 h, which is confirmed Figure 4(b).

The formation of δ -phase was suppressed at heat treatment times below 10 h by the absence of Nb segregation after HIP post-processing. With additional heat treatment times, the amount of δ -phase increased rapidly, reaching a volume fraction of (11.1 ± 3.5) % after 50 h. Unlike the clustered morphologies observed in the as-deposited condition, however, a rather uniform distribution of thin needles throughout the microstructure was observed, as shown in Figure 6(e). With increasing times, the δ -phase volume fraction continued to increase, albeit at a lower rate, and reached a peak of (13.6 ± 2.3) % at a time of 500 h. With additional times, a slight decrease in δ -phase volume fraction was observed, falling to (11.9 ± 1.6) % after 1000 h.

3.3 Evolution of δ -phase in Inconel 625 containing Z-phase and η -nitrides

Slight changes in selected alloying elements impact the secondary phases which form during AM processing [11, 12, 26, 35]. The formation of Z-phase and η -nitrides were promoted in the as-deposited low Fe Inconel 625, which contained a Si mass fraction of 0.39 % and Ti mass fraction of 0.03 %. The presence of these nitrides, in addition to the lower Nb mass fraction in the alloy, led to a decrease in the mass fraction of Nb in the interdendritic regions, as shown in Figure 7(a). However, the remaining Nb mass fractions in solution were still sufficient to promote the precipitation of secondary phases in the interdendritic regions in the early stages of heat treatment, as shown in Figure 8.

The general size and morphology of these secondary phases remained rather unchanged from those observed in the as-deposited condition through the first 10 h of heat treatment as shown in Figure 8(a)-(d). Growth of these nitrides, which were identified as Z-phase and η -nitrides in Figure 9(a), primarily occurred in the interdendritic regions and led to a drop in the Nb mass fraction to (2.95 ± 0.25) %. After 10 h, the volume fraction of the precipitates reached (7.6 ± 0.3) %, as shown in Figure 10(a). Some isolated δ -phase needles were observed, as indicated by the arrows in Figure 8, but fell far below the volume fractions observed in the alloy with MN nitrides present. After approximately 10 h, the total volume fraction of nitrides stabilized within the uncertainty of the measurement for the remainder of the heat treatment. The chain-like morphologies of nitrides first observed in the as-deposited condition evolved into a blocky

appearance, and the individual nitrides became more separated as the heat treatment time exceeded 50 h, as shown in Figure 8(e).

As the nitrides took on this blocky appearance after the 10 h heat treatment, η -nitrides and δ -phase needles began to grow at the expense of Z-phase, as shown in Figure 9(a). Between 10 h and 50 h, the Z-phase disappeared and was replaced by η -nitrides and δ -phase. Although the precipitation of δ -phase was detected as early as 0.5 h, as shown in Figure 8(a), the volume fraction remained low for the duration of the 1000 h heat treatment. More isolated δ -phase needles are observed with increasing heat treatment time, and the δ -phase volume fraction reached $(1.5 \pm 1.0) \%$. Further heat treatment time has little effect on δ -phase growth, as the volume fraction stayed at or below roughly 2 % for the duration of the heat treatment.

After HIP post-processing, the Z-phase and η -nitrides present in the as-deposited materials remained, but their volume fraction increased to $(2.6 \pm 0.7) \%$, and no δ -phase was detected. The Z-phase and η -nitrides identified in Figure 9(b) became coarser after HIP post-processing, as shown by comparing Figure 1(a) and Figure 1(c), and maintained this coarse and blocky appearance in the early stages of heat treatment, as shown in Figure 11. After short heat treatment times, an immediate increase was observed in the volume fraction of Z-phase and η -nitrides, as shown in Figure 10(a), but quickly stabilized within measurement uncertainty. No appreciable differences for the duration of the heat treatment were observed in the nitride volume fraction after a heat treatment time of approximately 1 h.

Similar to the as-deposited condition, the Z-phase present after HIP post-processing began dissolving after a heat treatment time of 10 h, as shown in Figure 9(b). More time, however, was needed to dissolve the Z-phase, which persisted up to a heat treatment time of 100 h. As Z-phase dissolved, η -nitrides and δ -phase volume fractions increased and consumed Nb gradually from the matrix, as shown in Figure 7(b). The δ -phase needles elongated with time but remained isolated, as shown in Figure 8. After an extended heat treatment of 1000 h, the volume fractions of η -nitrides and δ -phase were $(4.6 \pm 0.6) \%$ and $(1.3 \pm 0.4) \%$, respectively.

3.4 Comparison between AM and wrought Inconel 625

The formation of δ -phase in wrought Inconel 625 provides a baseline comparison for the response of AM materials to similar heat treatment temperatures. In the as-received condition, a representative wrought Inconel 625 plate with a Nb mass fraction of $(3.25 \pm 0.12) \%$ contained η -carbides (M_6C) and $M(C,N)$ carbonitrides dispersed along grain boundaries at a volume fraction

of approximately 2 %. Figure 12 shows that these phases persist through the heat treatment times of up to 1000 h. Along with the presence of these carbides, needle-like δ -phase precipitates also form and evolve with increasing times, as shown in Figure 12 and Figure 13. Heat treatment times between 10 h and 50 h are needed to produce a δ -phase volume fraction of approximately $(3.8 \pm 3.5) \%$, as shown in Figure 12(b). After 1000 h, the δ -phase volume fraction reaches $(6.2 \pm 2.4) \%$. The morphology of δ -phase changed over time, starting as relatively short, thin needles and evolving after times of 500 h and 1000 h to thin, longer needles, as shown in Figure 13(c) and Figure 13(d), respectively.

A comparison of the measured and calculated Nb mass fractions in γ along with the corresponding carbide/nitride and δ -phase volume fractions in the AM and wrought materials after 1000 h is shown in Table 4. All measured Nb mass fractions reached similar values, regardless of initial alloy composition, elemental segregation, phase composition, or processing route. These values closely match those predicted under equilibrium conditions. However, the distribution of excess Nb in precipitates varies significantly among the different materials. The relatively high nitrogen contents of the AM materials led to the formation of higher measured nitride volume fractions compared to the carbide fraction in the wrought material containing little nitrogen. Since the low Fe material contained a higher volume fraction of nitrides that consumed Nb, insufficient Nb remained to promote δ -phase precipitation. Meanwhile, the nitrides in high Fe material both consumed less Nb and constituted a lower volume fraction, leading to high volume fractions of δ -phase precipitation. Although the wrought Inconel 625 contains Nb-containing carbides, the relatively low volume fraction resulted in sufficient Nb available to form δ -phase, where an intermediate volume fraction between the AM materials was measured.

4. Summary and Conclusions

The type and volume fraction of precipitates resulting from minor changes in Inconel 625 alloy composition influenced the amount of Nb available to promote δ -phase formation during isothermal heat treatments at 870 °C. Alloy compositions favoring the formation of a large volume fraction of Nb-containing precipitates reduced the source of Nb necessary for δ -phase formation. Altering δ -phase precipitation was demonstrated by isothermally heat treating two additively manufactured Inconel 625 alloys with variations in minor alloy elements for 1000 h and comparing with wrought material. Nitrogen promoted the precipitation of various nitrides including Z-phase,

η -nitrides, and MN nitrides depending on alloy composition in additively manufactured materials, while η -carbides and M(C,N) carbonitrides were present in wrought material. The as-deposited and hot isostatically pressed initial conditions were also evaluated to probe the influence of elemental segregation on δ -phase formation. The following are the main conclusions:

1. After 1000 h at 870 °C, an additively manufactured alloy with niobium-rich Z-phase and η -nitrides formed a δ -phase volume fraction less than 2 %, while the alloy with only titanium-rich MN nitrides formed between 10 % and 12 % δ -phase. The wrought material containing η -carbides and M(C,N) carbonitrides produced an intermediate δ -phase volume fraction of (6.2 ± 2.4) %.
2. Elemental segregation accelerated δ -phase formation due to the local enrichment of niobium compared to homogenized alloys of the same composition. In the as-deposited alloy forming approximately 10 % to 12 % volume fraction δ -phase, the precipitation can be quantified as early as 0.5 h of heat treatment. Heat treatments between 10 h and 50 h are needed before appreciable amounts of δ -phase are quantified in the hot isostatically pressed counterpart. Similarly, approximately 50 h and 500 h are needed for the as-deposited and hot isostatically pressed conditions, respectively, in the alloy containing Z-phase and η -nitrides.
3. The effects of elemental segregation in additively manufactured Inconel 625 were only relevant in the early stages of heat treatment. Prolonged exposure at 870 °C eventually led to similar δ -phase volume fractions in each alloy despite beginning in the as-deposited or hot isostatically pressed condition. In the alloy containing Z-phase and η -nitrides, the measured volume fractions are (1.7 ± 0.3) % and (1.3 ± 0.4) % for the as-deposited and hot isostatically pressed conditions, respectively, compared to (10.0 ± 2.9) % and (11.9 ± 1.6) % in the alloy with MN nitrides.
4. After prolonged heat treatments, the niobium in the γ -matrix reached a nearly identical mass fraction in all Inconel 625 alloys regardless of initial alloy composition, secondary phase fractions, chemical homogeneity, or processing route. In the as-deposited conditions, the measured Nb mass fractions were (2.39 ± 0.13) % and (2.34 ± 0.13) % for the low and high Fe alloys, respectively, compared to (2.39 ± 0.20) % and (2.37 ± 0.16) % for the hot isostatically pressed condition. Similarly, (2.45 ± 0.25) % was measured in the wrought Inconel 625.

5. The available Nb in solution dictated the amount of δ -phase that formed in Inconel 625 and was determined by the type and volume fraction of nitrides present in the microstructure prior to heat treatment. An additively manufactured alloy containing Ti-rich MN nitrides left much of the Nb in solution, allowing for δ -phase to form in volume fractions twice that of wrought material. In the other alloy, Z-phase and η -nitrides consumed more of the available Nb and suppressed δ -phase formation to a volume fraction 3 times less than wrought material.

Acknowledgements

The authors would like to acknowledge Cesar Ballester of Verder Scientific Inc. for detailed chemistry analysis of materials.

References

- [1] S. Floreen, G.E. Fuchs, W.J. Yang, The metallurgy of alloy 625, in: 3rd International Special Emphasis Symposium on Superalloys 718, 625, 706 and Various Derivatives, Pittsburgh, Pa, 1994, pp. 13-37.
- [2] H. Okamoto, Nb-Ni (Niobium–Nickel), *Journal of Phase Equilibria and Diffusion*, 29 (2008) 210-210.
- [3] S. Azadian, L.-Y. Wei, R. Warren, Delta phase precipitation in Inconel 718, *Materials Characterization*, 53 (2004) 7-16.
- [4] M.J. Anderson, J. Benson, J.W. Brooks, B. Saunders, H.C. Basoalto, Predicting Precipitation Kinetics During the Annealing of Additive Manufactured Inconel 625 Components, *Integrating Materials and Manufacturing Innovation*, 8 (2019) 154-166.
- [5] V. Shankar, K. Bhanu Sankara Rao, S.L. Mannan, Microstructure and mechanical properties of Inconel 625 superalloy, *Journal of Nuclear Materials*, 288 (2001) 222-232.
- [6] M. Sundararaman, P. Mukhopadhyay, S. Banerjee, Precipitation of the δ -Ni₃Nb phase in two nickel base superalloys, *Metallurgical Transactions A*, 19 (1988) 453-465.
- [7] J. Mitra, S. Banerjee, R. Tewari, G.K. Dey, Fracture behavior of Alloy 625 with different precipitate microstructures, *Materials Science and Engineering: A*, 574 (2013) 86-93.
- [8] J.J. deBarbadillo, S.K. Mannan, Alloy 718 for Oilfield Applications, *JOM*, 64 (2012) 265-270.
- [9] T. DebRoy, H.L. Wei, J.S. Zuback, T. Mukherjee, J.W. Elmer, J.O. Milewski, A.M. Beese, A. Wilson-Heid, A. De, W. Zhang, Additive manufacturing of metallic components – Process, structure and properties, *Progress in Materials Science*, 92 (2018) 112-224.
- [10] T. Keller, G. Lindwall, S. Ghosh, L. Ma, B.M. Lane, F. Zhang, U.R. Kattner, E.A. Lass, J.C. Heigel, Y. Idell, M.E. Williams, A.J. Allen, J.E. Guyer, L.E. Levine, Application of finite element, phase-field, and CALPHAD-based methods to additive manufacturing of Ni-based superalloys, *Acta Materialia*, 139 (2017) 244-253.
- [11] Z.R. Khayat, T.A. Palmer, Impact of iron composition on the properties of an additively manufactured solid solution strengthened nickel base alloy, *Materials Science and Engineering: A*, 718 (2018) 123-134.

- [12] J.S. Zuback, P. Moradifar, Z. Khayat, N. Alem, T.A. Palmer, Impact of chemical composition on precipitate morphology in an additively manufactured nickel base superalloy, *Journal of Alloys and Compounds*, 798 (2019) 446-457.
- [13] Y.L. Hu, X. Lin, X.B. Yu, J.J. Xu, M. Lei, W.D. Huang, Effect of Ti addition on cracking and microhardness of Inconel 625 during the laser solid forming processing, *Journal of Alloys and Compounds*, 711 (2017) 267-277.
- [14] F. Zhang, L.E. Levine, A.J. Allen, M.R. Stoudt, G. Lindwall, E.A. Lass, M.E. Williams, Y. Idell, C.E. Campbell, Effect of heat treatment on the microstructural evolution of a nickel-based superalloy additive-manufactured by laser powder bed fusion, *Acta Materialia*, 152 (2018) 200-214.
- [15] G. Lindwall, C.E. Campbell, E.A. Lass, F. Zhang, M.R. Stoudt, A.J. Allen, L.E. Levine, Simulation of TTT Curves for Additively Manufactured Inconel 625, *Metallurgical and Materials Transactions A*, 50 (2019) 457-467.
- [16] E.A. Lass, M.R. Stoudt, M.E. Williams, M.B. Katz, L.E. Levine, T.Q. Phan, T.H. Gnaeupel-Herold, D.S. Ng, Formation of the Ni₃Nb δ -Phase in Stress-Relieved Inconel 625 Produced via Laser Powder-Bed Fusion Additive Manufacturing, *Metallurgical and Materials Transactions A*, 48 (2017) 5547-5558.
- [17] E.A. Lass, M.R. Stoudt, M.B. Katz, M.E. Williams, Precipitation and dissolution of δ and γ'' during heat treatment of a laser powder-bed fusion produced Ni-based superalloy, *Scripta Materialia*, 154 (2018) 83-86.
- [18] M.R. Stoudt, E.A. Lass, D.S. Ng, M.E. Williams, F. Zhang, C.E. Campbell, G. Lindwall, L.E. Levine, The Influence of Annealing Temperature and Time on the Formation of δ -Phase in Additively-Manufactured Inconel 625, *Metallurgical and Materials Transactions A*, 49 (2018) 3028-3037.
- [19] C.C. Silva, V.H.C. de Albuquerque, E.M. Miná, E.P. Moura, J.M.R.S. Tavares, Mechanical Properties and Microstructural Characterization of Aged Nickel-based Alloy 625 Weld Metal, *Metallurgical and Materials Transactions A*, 49 (2018) 1653-1673.
- [20] T. Dai, R.A. Wheeling, K. Hartman-Vaeth, J.C. Lippold, Precipitation behavior and hardness response of Alloy 625 weld overlay under different aging conditions, *Welding in the World*, 63 (2019) 1087-1100.
- [21] Y. Mu, C. Wang, W. Zhou, L. Zhou, Effect of Nb on δ Phase Precipitation and the Tensile Properties in Cast Alloy IN625, *Metals*, 8 (2018) 86.
- [22] J.N. DuPont, J.C. Lippold, S.D. Kiser, *Welding metallurgy and weldability of nickel-base alloys*, John Wiley & Sons, Hoboken, NJ, 2011.
- [23] J.N. DuPont, A.R. Marder, M.R. Notis, C.V. Robino, Solidification of Nb-bearing superalloys: Part II. Pseudoternary solidification surfaces, *Metallurgical and Materials Transactions A*, 29 (1998) 2797-2806.
- [24] M. Cieslak, T. Headley, A. Romig, T. Kollie, A melting and solidification study of alloy 625, *Metallurgical Transactions A*, 19 (1988) 2319-2331.
- [25] J.N. DuPont, Solidification of an alloy 625 weld overlay, *Metallurgical and Materials Transactions A*, 27 (1996) 3612-3620.
- [26] J.S. Zuback, A.D. Iams, F. Zhang, L.A. Giannuzzi, T.A. Palmer, Stable nitride precipitation in additively manufactured nickel superalloys, *Journal of Alloys and Compounds*, 910 (2022) 164918.
- [27] A. Banerjee, M.-R. He, W.D. Musinski, P.A. Shade, M.E. Cox, E.J. Schwalbach, K.J. Hemker, Effect of stress-relief heat treatments on the microstructure and mechanical response of

- additively manufactured IN625 thin-walled elements, *Materials Science and Engineering: A*, 846 (2022) 143288.
- [28] M.-R. He, A. Banerjee, C.J. Marvel, S. Price, I. McCue, E.J. Schwalbach, K.J. Hemker, Strong Impact of Minor Elements on the Microstructural Evolution of an Additively Manufactured Inconel 625 Alloy, *Metallurgical and Materials Transactions A*, 53 (2022) 2926-2942.
- [29] ASTM B443-19, Standard specification for Nickel-Chromium-Molybdenum-Columbium alloy and Nickel-Chromium-Molybdenum-Silicon alloy plate, sheet, and strip, ASTM International, West Conshohocken, PA, 2019.
- [30] J.O. Andersson, T. Helander, L. Höglund, P. Shi, B. Sundman, Thermo-Calc & DICTRA, computational tools for materials science, *Calphad*, 26 (2002) 273-312.
- [31] Thermo-Calc Software TCNI8 Ni-alloys database, (Accessed 6 June 2023).
- [32] ASTM F3056-14, Standard specification for additive manufacturing nickel alloy (UNS N06625) with powder bed fusion, ASTM International, West Conshohocken, PA, 2021.
- [33] I. Levin, NIST Inorganic Crystal Structure Database (ICSD), in, National Institute of Standards and Technology, 2018.
- [34] ASTM E562-08, Standard test method for determining volume fraction by systematic manual point count, ASTM International, West Conshohocken, PA, 2008.
- [35] A. Kreitzberg, V. Brailovski, Effect of Fe and C Contents on the Microstructure and High-Temperature Mechanical Properties of IN625 Alloy Processed by Laser Powder Bed Fusion, *Materials*, 15 (2022) 6606.

Figures

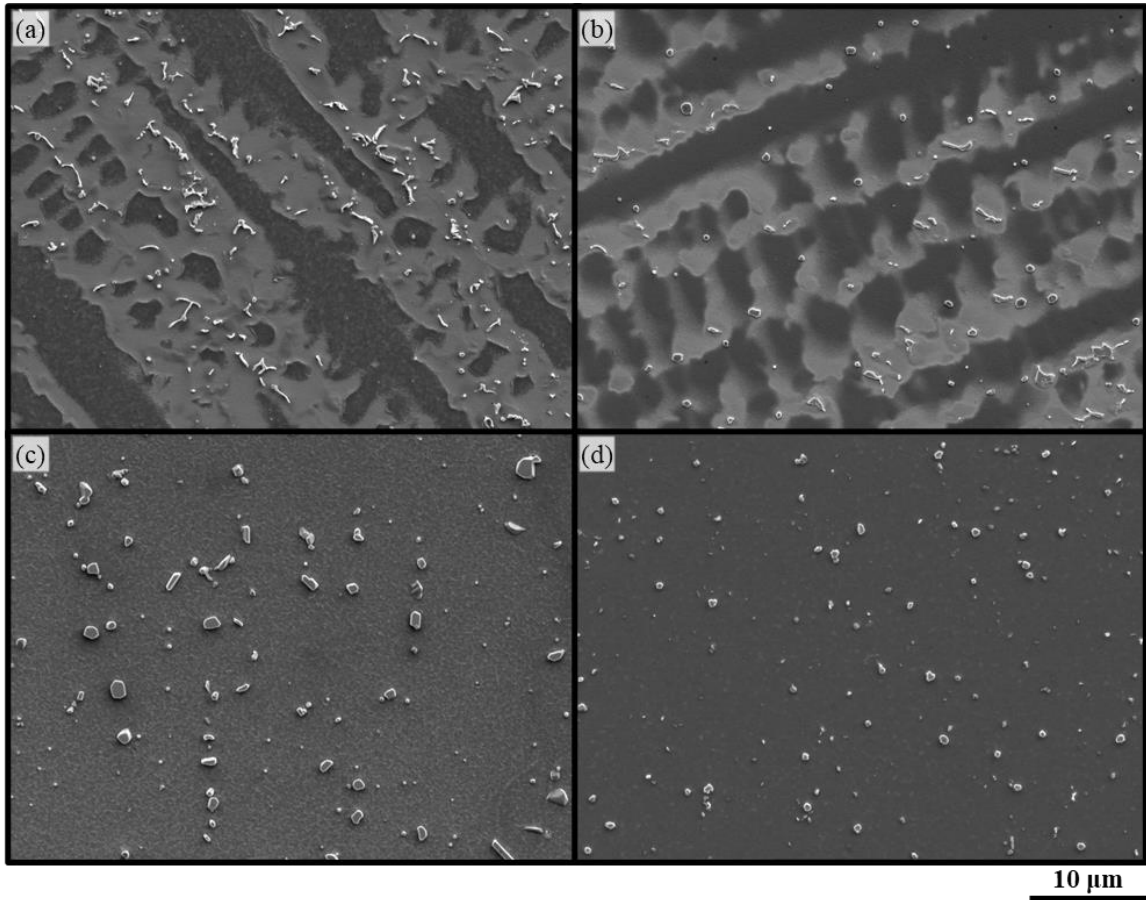


Figure 1. Secondary electron SEM micrographs of the (a) as-deposited low Fe, (b) as-deposited high Fe, (c) HIP low Fe, and (d) HIP high Fe Inconel 625 prior to isothermal heat treatment at 870 °C.

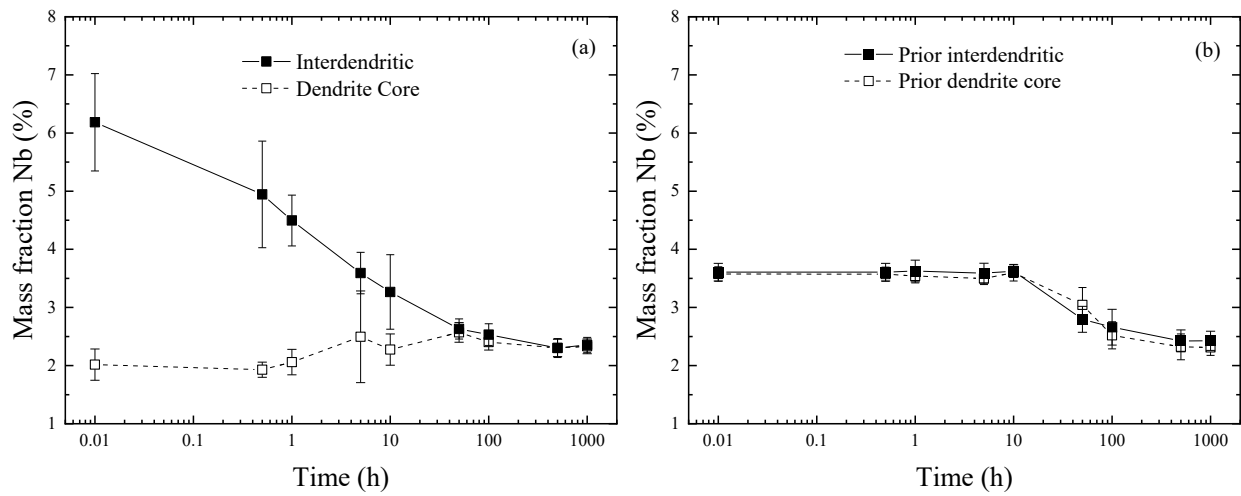


Figure 2. Measured average mass fractions of Nb in the (a) as-deposited and (b) HIP high Fe Inconel 625 alloys containing MN nitrides as a function of heat treatment time at 870 °C. Error bars represent the standard deviation.

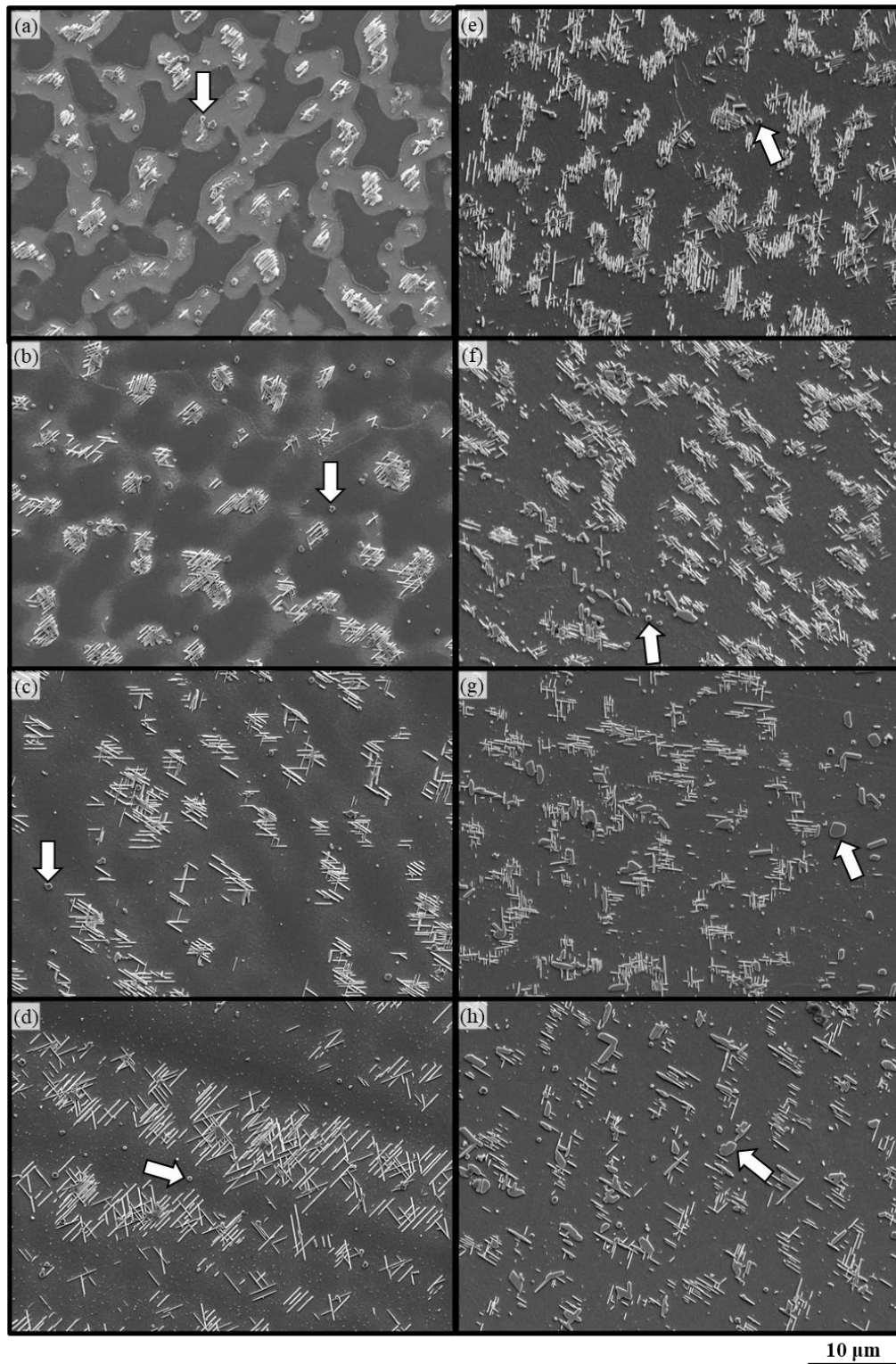


Figure 3. Secondary electron SEM micrographs of precipitate evolution in the as-deposited high Fe Inconel 625 containing MN nitrides after heat treatment at 870 °C for (a) 0.5 h, (b) 1 h, (c) 5 h, (d) 10 h, (e) 50 h, (f) 100 h, (g) 500 h, (h) 1000 h. MN nitrides are indicated by arrows.

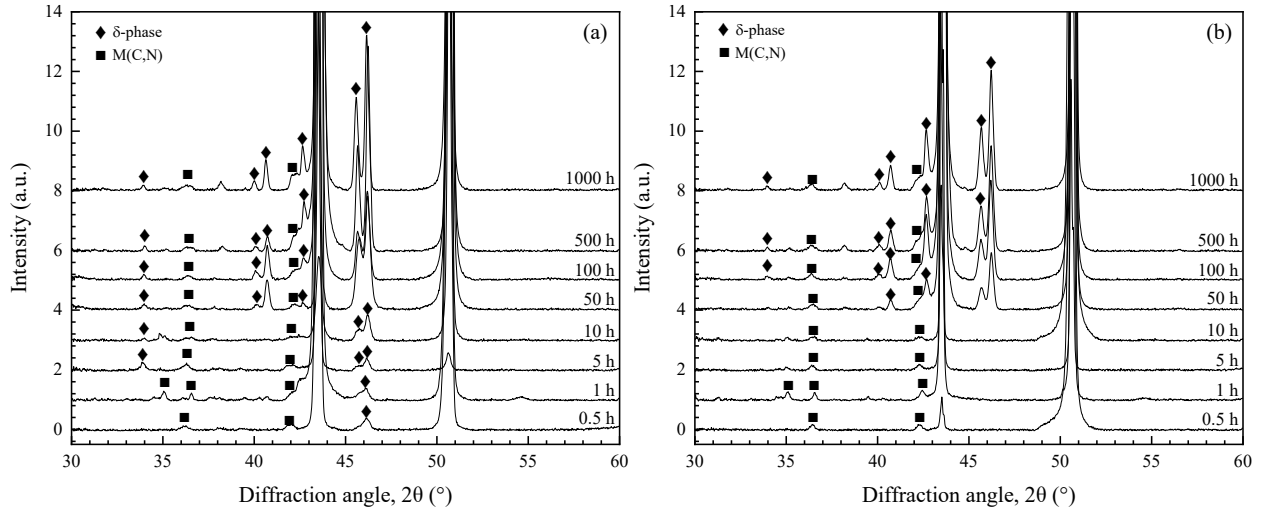


Figure 4. X-ray diffraction profiles for the (a) as-deposited and (b) HIP high Fe Inconel 625 alloys containing MN nitrides after isothermal heat treatment at 870 °C.

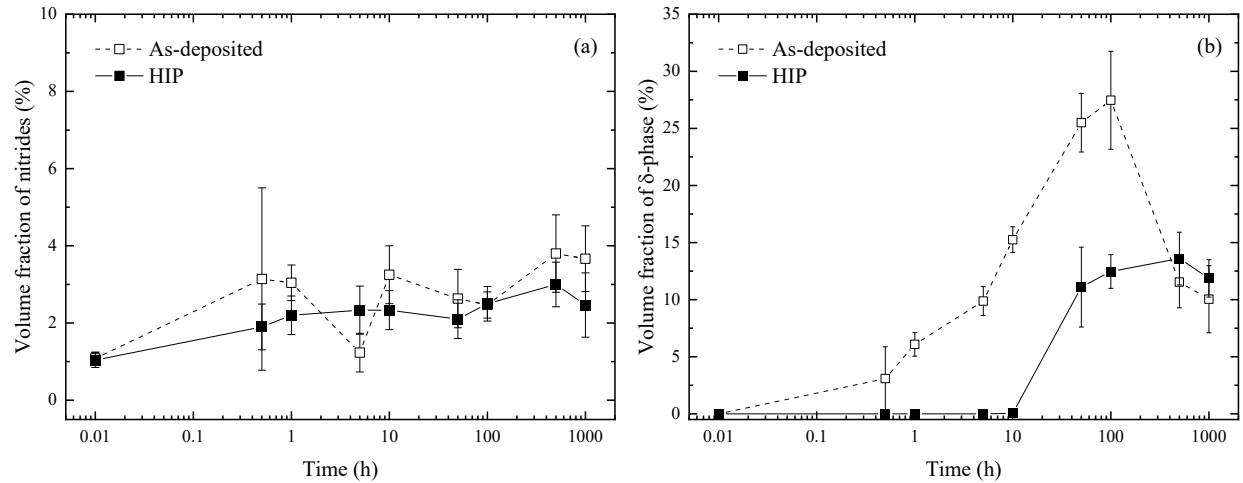


Figure 5. A comparison between the measured (a) nitride and (b) δ -phase volume fractions in the high Fe Inconel 625 alloys containing MN nitrides after different heat-treating times at 870 °C. Error bars represent the standard deviation.

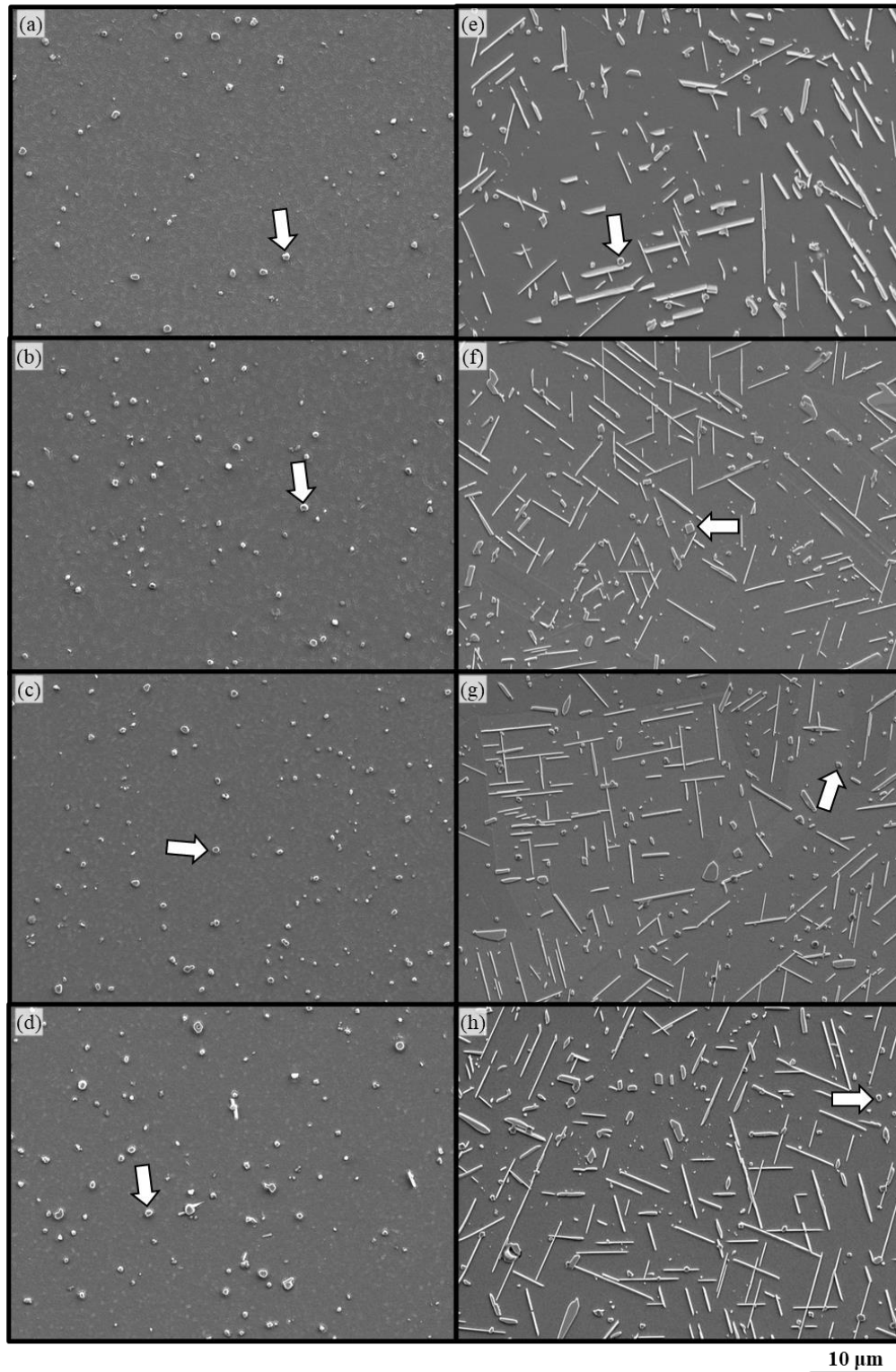


Figure 6. Secondary electron SEM micrographs of precipitate evolution in the HIP high Fe Inconel 625 containing MN nitrides after heat treatment at 870 °C for (a) 0.5 h, (b) 1 h, (c) 5 h, (d) 10 h, (e) 50 h, (f) 100 h, (g) 500 h, (h) 1000 h. MN nitrides are indicated by arrows.

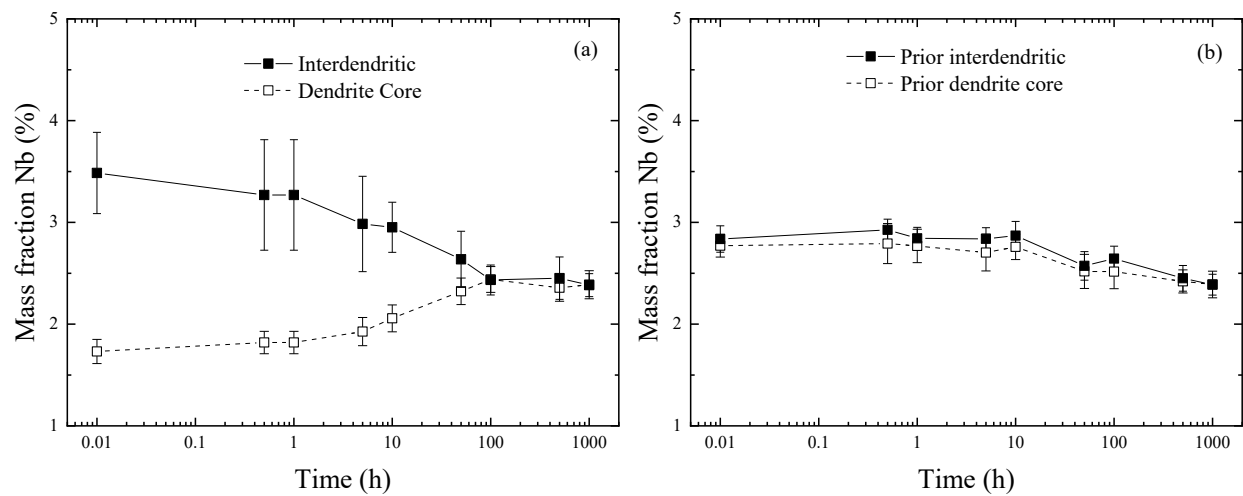


Figure 7. Measured average mass fractions of Nb in the (a) as-deposited and (b) HIP low Fe Inconel 625 materials containing Z-phase and η -nitrides as a function of heat treatment time at 870 °C. Error bars represent the standard deviation.

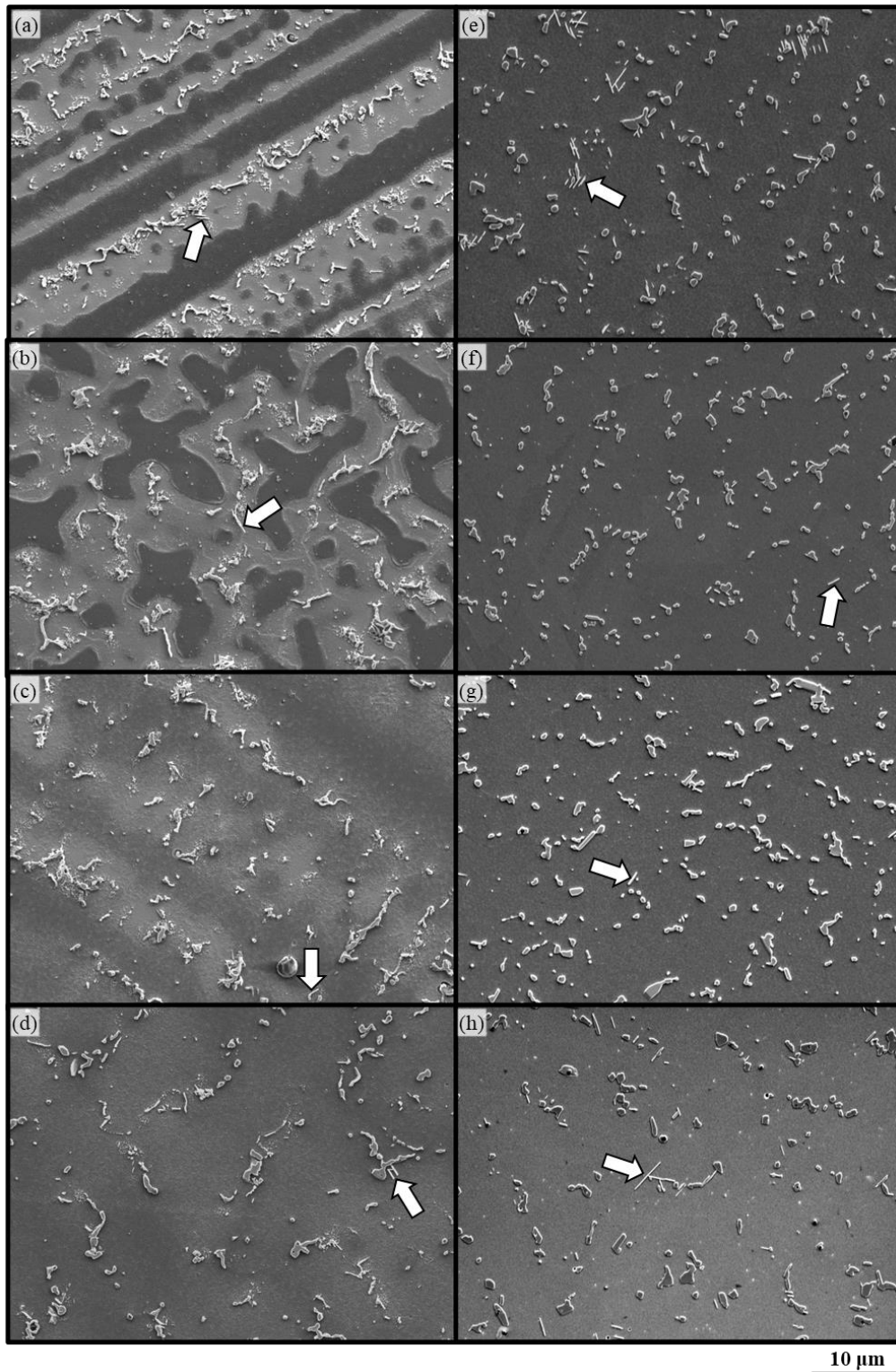


Figure 8. Secondary electron SEM micrographs of precipitate evolution in the as-deposited low Fe Inconel 625 containing Z-phase and η -nitrides after heat treatment at 870 °C for (a) 0.5 h, (b) 1 h, (c) 5 h, (d) 10 h, (e) 50 h, (f) 100 h, (g) 500 h, (h) 1000 h. δ -phase is indicated by arrows.

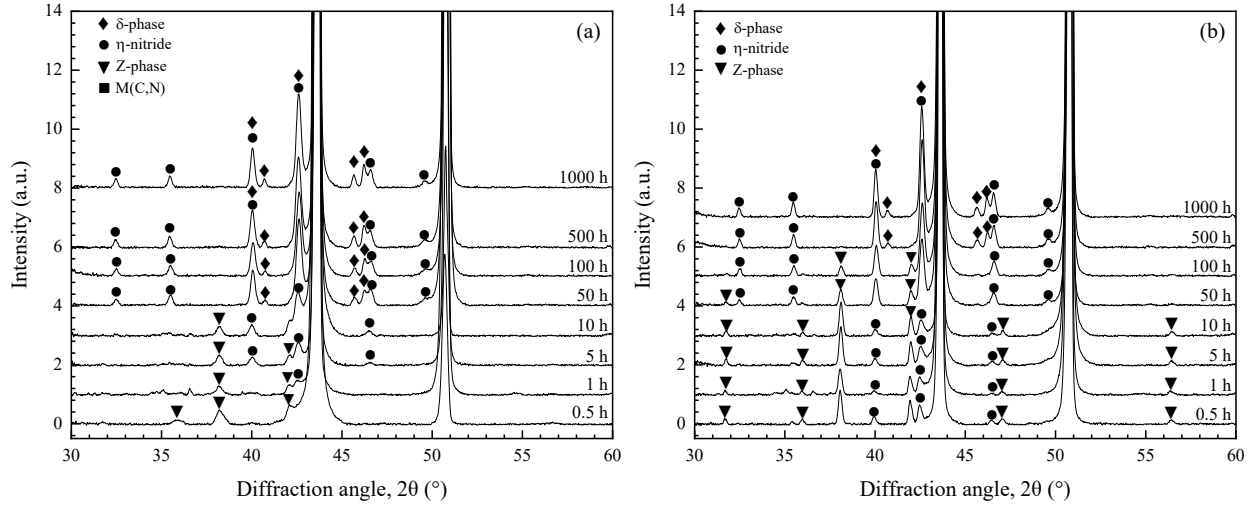


Figure 9. X-ray diffraction profiles for the (a) as-deposited and (b) HIP low Fe Inconel 625 materials containing Z-phase and η -nitrides after isothermal heat treatment at 870 °C.

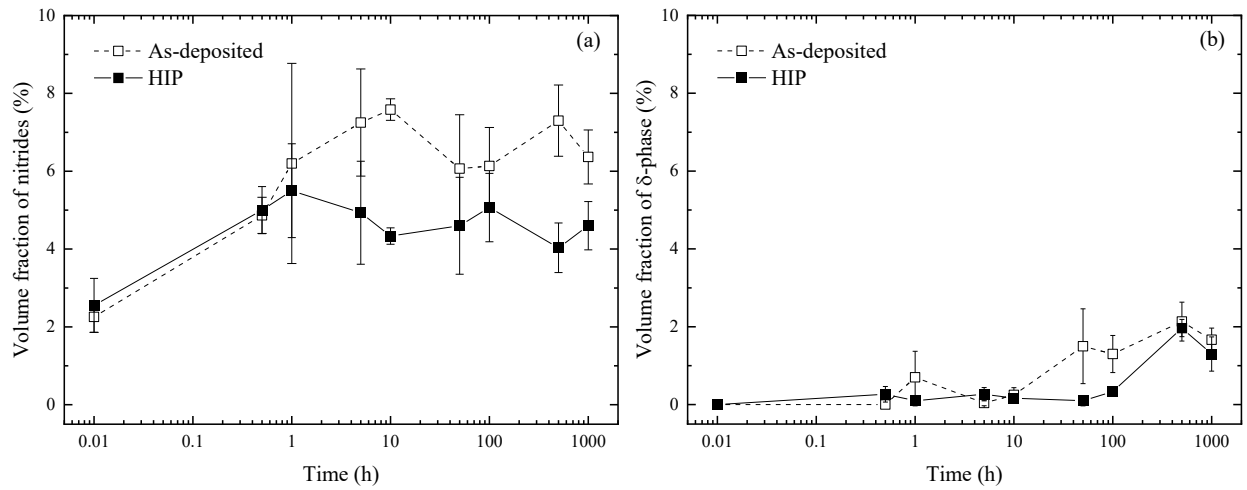


Figure 10. A comparison between the measured (a) nitride and (b) δ -phase volume fractions in HIP low Fe Inconel 625 alloys containing Z-phase and η -nitrides different heat-treating times at 870 °C using the point count method. Error bars represent the standard deviation.

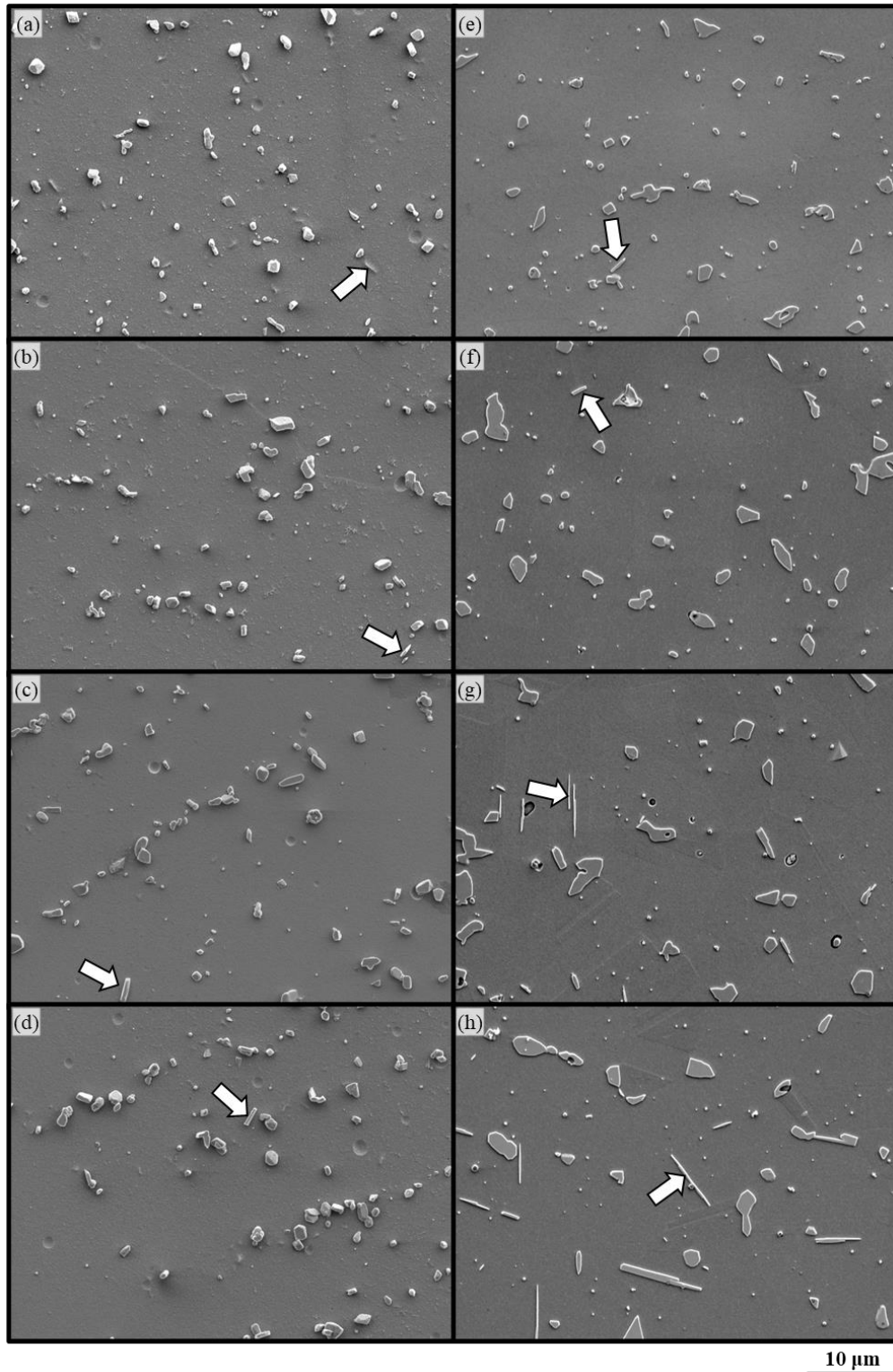


Figure 11. Secondary electron SEM micrographs of precipitate evolution in the HIP low Fe Inconel 625 containing Z-phase and η -nitrides after heat treatment at 870 °C for (a) 0.5 h, (b) 1 h, (c) 5 h, (d) 10 h, (e) 50 h, (f) 100 h, (g) 500 h, (h) 1000 h. δ -phase is indicated by arrows.

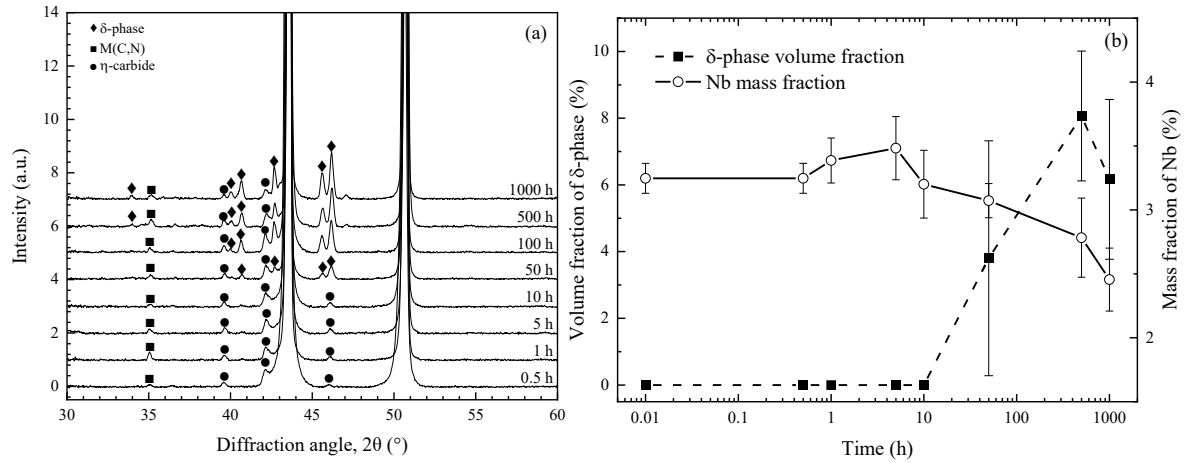


Figure 12. (a) X-ray diffraction profiles and (b) measured δ -phase volume fractions and Nb mass fractions for the wrought Inconel 625 material after isothermal heat treatment at 870 °C. Error bars represent the standard deviation.

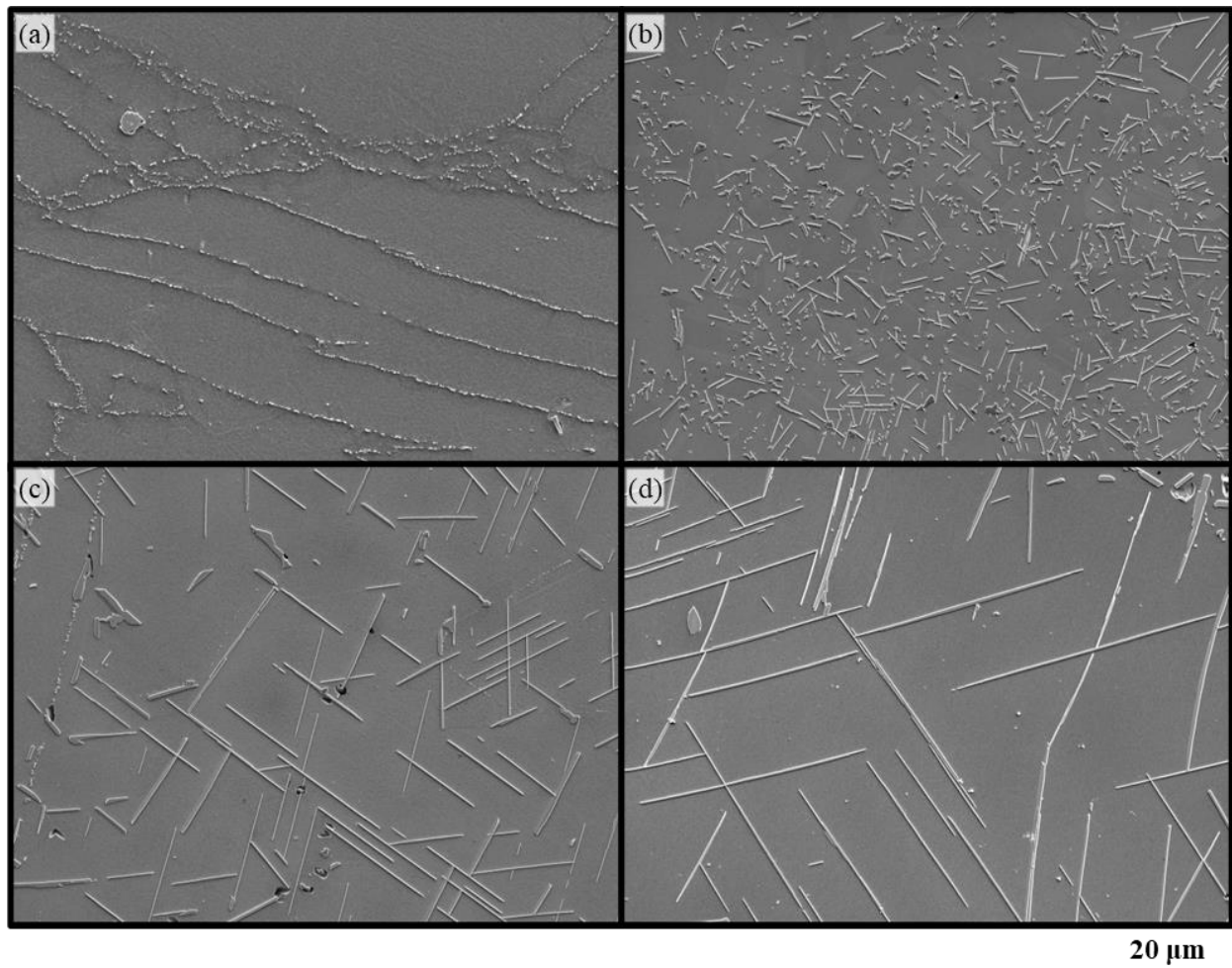


Figure 13. Secondary electron SEM micrographs of precipitate evolution in the wrought Inconel 625 after heat treatment at 870 °C for (a) 0.5 h, (b) 50 h (c) 500 h and (d) 1000 h.

Tables

Table 1. Measured mass fractions (in %) of AM and wrought Inconel 625 alloys with standard specification [29].

Material	Cr	Fe	Mn	Mo	Nb	Si	Ti	C	N	O
Low Fe	21.6	1.07	0.28	8.83	3.47	0.39	0.033	0.009	0.127	0.030
High Fe	21.5	4.14	0.085	8.96	4.11	0.051	0.21	0.006	0.080	0.007
Wrought	22.3	3.11	0.08	8.86	3.41	0.17	0.21	0.021	0.023	0.005
ASTM B443-19	20 to 23	<5	<0.5	8 to 10	3.15 to 4.15	<0.5	<0.4	<0.1	-	-

Table 2. Summary of local mass fraction (in %) variations of metallic elements in the γ -matrix of as-deposited and HIP Inconel 625 alloys. Locations in the HIP conditions correspond to regions in the microstructure that are assumed to be dendrite cores or interdendritic areas prior to HIP based on the locations of precipitates.

Location	Ni	Cr	Fe	Mn	Mo	Nb	Si	Ti
<i>Low Fe – As-deposited</i>								
<i>Dendrite core</i>	66.3 ± 0.31	22.4 ± 0.16	1.05 ± 0.04	0.42 ± 0.06	7.75 ± 0.13	1.73 ± 0.12	0.32 ± 0.04	0.03 ± 0.02
<i>Interdendritic</i>	64.1 ± 0.47	21.6 ± 0.27	0.98 ± 0.11	0.46 ± 0.10	8.90 ± 0.22	3.49 ± 0.40	0.45 ± 0.04	0.10 ± 0.02
<i>Low Fe - HIP</i>								
<i>Dendrite core</i>	64.7 ± 0.24	22.1 ± 0.14	1.02 ± 0.07	0.43 ± 0.08	8.45 ± 0.12	2.84 ± 0.13	0.43 ± 0.03	0.02 ± 0.03
<i>Interdendritic</i>	64.7 ± 0.32	22.1 ± 0.17	1.00 ± 0.09	0.46 ± 0.09	8.43 ± 0.21	2.77 ± 0.11	0.44 ± 0.04	0.01 ± 0.02
<i>High Fe – As-deposited</i>								
<i>Dendrite core</i>	63.9 ± 0.43	21.4 ± 0.14	4.44 ± 0.11	0.09 ± 0.09	7.90 ± 0.22	2.02 ± 0.27	0.10 ± 0.03	0.11 ± 0.03
<i>Interdendritic</i>	59.3 ± 0.71	20.3 ± 0.34	3.82 ± 0.11	0.10 ± 0.08	10.1 ± 0.28	6.19 ± 0.84	0.13 ± 0.03	0.10 ± 0.05
<i>High Fe - HIP</i>								
<i>Dendrite core</i>	61.9 ± 0.30	21.4 ± 0.18	4.18 ± 0.10	0.09 ± 0.06	8.72 ± 0.13	3.57 ± 0.12	0.09 ± 0.02	0.11 ± 0.11
<i>Interdendritic</i>	61.9 ± 0.42	21.3 ± 0.21	4.18 ± 0.09	0.09 ± 0.08	8.70 ± 0.22	3.61 ± 0.15	0.10 ± 0.03	0.11 ± 0.06

Table 3. Summary of the crystal structures and chemical compositions of nitrides identified in the low and high Fe Inconel 625 AM alloys [26].

Material	Condition	Phase	Structure	Lattice parameter (Å)	Composition in mass fraction (%)						
					Cr	Mo	Nb	Ni	Si	Ti	N
Low Fe	As-deposited	MN	FCC (Fm $\bar{3}$ m)	$a = 4.345 \pm 0.002$	3.9	-	91.1	-	-	-	5.0
		η	Diamond cubic (Fd $\bar{3}$ m)	$a = 11.011 \pm 0.075$	12.7	15.3	35.9	32.3	2.6	-	1.2
		Z-phase	Tetragonal (P4/nmm)	$a = 3.072 \pm 0.001$ $c = 7.532 \pm 0.004$	22.6	17.2	54.2	3.0	-	-	3.0
	HIP	η	Diamond cubic (Fd $\bar{3}$ m)	$a = 11.02 \pm 0.018$	Not measured						
		Z-phase	Tetragonal (P4/nmm)	$a = 3.040 \pm 0.0004$ $c = 7.479 \pm 0.003$	22.3	17.9	55.2	0.7	-	-	4.0
	High Fe	As-deposited	MN	FCC (Fm $\bar{3}$ m)	$a = 4.299 \pm 0.003$	8.6	-	45.1	-	-	33.0
HIP		MN	FCC (Fm $\bar{3}$ m)	$a = 4.270 \pm 0.002$	1.1	-	27.4	-	-	57.7	13.8
		MN	FCC (Fm $\bar{3}$ m)		3.0	-	45.2	-	-	40.7	11.1

Table 4. Comparison of the measured and calculated equilibrium Nb mass fractions in the γ -matrix and volume fractions of precipitates in the AM and wrought Inconel 625 materials after 1000 h of heat treatment at 870 °C.

Material	Condition	Nb mass fraction (%)		Carbide/nitride volume fraction (%)		δ -phase volume fraction (%)	
		Measured	Equilibrium	Measured	Equilibrium	Measured	Equilibrium
Low Fe	As-built	2.39 ± 0.13	2.30 ± 0.06	6.4 ± 0.7	1.6 ± 0.1	1.7 ± 0.3	1.2 ± 0.2
Low Fe	HIP	2.39 ± 0.20		4.6 ± 0.6		1.3 ± 0.4	
High Fe	As-built	2.34 ± 0.13	2.51 ± 0.07	3.7 ± 0.8	0.6 ± 0.1	10.0 ± 2.9	4.4 ± 0.2
High Fe	HIP	2.37 ± 0.16		2.5 ± 0.8		11.9 ± 1.6	
Wrought	As-received	2.45 ± 0.25	2.19 ± 0.07	0.9 ± 0.7	0.3 ± 0.1	6.2 ± 2.4	4.4 ± 0.2